Analysis of noise in Magneto-Electric thin layer composites used as magnetic sensor

Xin Zhuang, Marc Lam Chok Sing, Christophe Cordier, Sébastien Saez, Christophe Dolabdjian, Jaydip Das, Junqi Gao, Jiefang Li, Dwight Viehland

Analysis of Noise in Magnetoelectric Thin-Layer Composites Used as Magnetic Sensors

Xin Zhuang, Marc Lam Chok Sing, Christophe Cordier, Sébastien Saez, Christophe Dolabdjian, Jaydip Das, Junqi Gao, Jiefang Li, and Dwight Viehland

***Abstract*—Taking advantage of magneto-elasto-electric interactions, new laminated composites of magnetostrictive and piezoelectric layers have been developed for highly sensitivity magnetoelectric (ME) sensors. The ME sensor design chosen in this study was based on long-type Metglas composites laminated together with piezoelectric fibers. In this paper, we analyze the expected limit of the magnetic noise of ME sensor versus its intrinsic characteristics and electronic setup. Theory calculations and experimental results are compared, and are well supported by noise measurements. Moreover, the presented results show very impressive performances in terms of the equivalent magnetic sensor noise. A 65 $\mathrm{pT}/\sqrt{\mathrm{Hz}}$ equivalent magnetic noise was achieved at 1 Hz, while reaching values as low as 70 $\mathrm{fT}/\sqrt{\mathrm{Hz}}$ near the ME resonant frequency.**

***Index Terms*—Equivalent magnetic noise, low-noise circuit, magnetoelectric effect, magnetoelectric (ME) charge coefficient.**

I. Introduction

MAGNETOSTRICTIVE/PIEZOELECTRIC laminate composites are known to produce a large magnetoelectric (ME) effect [1]. Conventional ME sensors have been fabricated by laminating a piezoelectric layer sandwiched between two magnetostrictive layers, e.g., Terfenol-D/PZT/Terfenol-D layers [2], [3]. Stresses in the magnetostrictive layers due to the magnetostriction are transferred via the intermediate epoxy resin to the piezoelectric layers, where they produce an electric charge due to the piezoelectric effect.

By using Metglas layers/PZT fiber laminate composites [3], more recent generations of ME composite sensors have been shown to have giant ME effects [4]. The vibration direction of the Metglas layer(s) is longitudinal, and subsequently the stresses on the PZT fibers are along the same direction. Therefore, interdigitatal (ID) electrodes on the two faces of the PZT fibers collect the electric charges as an output signal. The fabrication technology will be described in more detail in latter sections.

The sensor detection capabilities are affected by intrinsic and extrinsic noise. Extrinsic noise sources exist in the environment, and they can probably be reduced by rejection techniques. However, the intrinsic noise is not able to be avoided: such as Johnson noise, and $1/f$ noise in the resistors and semiconductors, in the detection circuit. Measurement circuitry and ME laminate design must both be considered for ME sensor performance optimization.

In the following sections, we shall analyze the detection circuit in the small signal regime. Noise source models will be described and used to analyze sensor performances. Experimental results and measurement conditions will also be presented in these sections in terms of charge coefficients, transfer functions, and noise levels. Furthermore, both small bandwidth and large bandwidth sensor performances will be compared with theoretical ones.

II. ME Sensors

ME sensors consist of magnetostrictive and piezoelectric glued layers. Metglas with high piezomagnetic coefficient, and PZT with high piezoelectric coefficient, were selected to obtain the highest ME response. This in turn resulted in high magnetic field sensitivity. First, we attached kapton insulating films with ID copper electrodes to both the top and bottom of five 200 μm thick commercial PZT fibers (CTS Wireless, Albuquerque, NM) using an epoxy resin. This allowed us to obtain the push-pull geometry [5]. This configuration consists of a longitudinally magnetized magnetic layer, and a piezoelectric layer symmetrically poled about its central nodal point in reverse directions along the longitudinal axis. This configuration offers a high ME coupling between the magnetic and electric layers. The dimension of each PZT fiber was 0.2 cm $\times$ 4.0 cm, and the distance between the electrodes was 850 μm. The Metglas foils were 25 μm thick (Metglas Inc., Conway, SC), had saturation magnetostrictions of about 27 ppm, and were cut to widths of about 1 cm so as to match the total width of the five PZT fibers. The length of the Metglas was 8 cm, which was chosen so as to obtain maximum flux concentration over the laminate structure. Metglas pieces were then stacked one on top of each other, bonded with epoxy resin, and were pressed using a hydraulic press to minimize the epoxy thickness in-between the Metglas foils. Metglas stacks with two, four, and six layers were then attached at the top and bottom of the ID electrode-PZT-ID electrode structure with epoxy, in order to obtain ME laminate layered structures. Fig. 1 shows: (a) schematic diagram and

X. Zhuang, M. Lam Chok Sing, C. Cordier, S. Saez, and C. Dolabdjian are with the Groupe de Recherche en Informatique, Image, Automatique et Instrumentation de Caen (GREYC), CNRS UMR 6072-ENSICAEN and the University of Caen, France 14050 Caen Cedex (e-mail: Xin.Zhuang@greyc.ensicaen.fr; M.Lam@greyc.ensicaen.fr; christophe.cordier@unicaen.fr; sebastien.saez@unicaen.fr; christophe.dolabdjian@unicaen.fr).

J. Das, J. Gao, J. Li, and D. Viehland are with the Department of Materials Science and Engineering, Virginia Polytechnic Institute and State University, Blacksburg, VA 24061 USA (e-mail: jaydip@vt.edu; junqi08@vt.edu; jiefang@mse.vt.edu; viehland@mse.vt.edu).

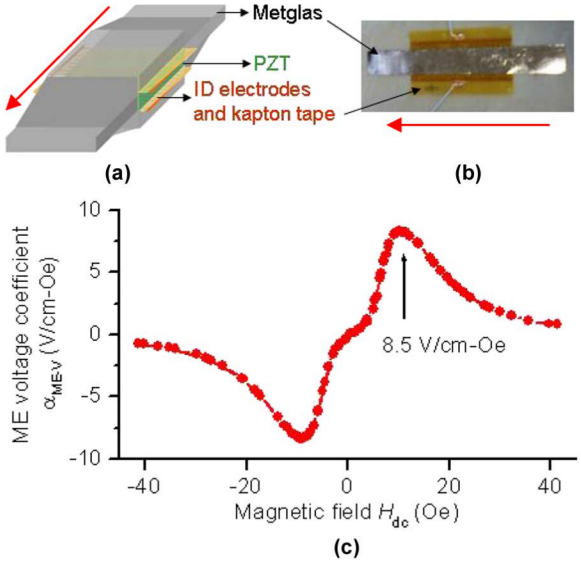

Fig. 1. (a) Schematic diagram and (b) a picture of the Metglas-PZT laminate structure. (c) Magneto-electric voltage coefficient $\alpha_{\mathrm{ME-V}}$ as a function of the static dc magnetic bias field H_{dc} for the laminate with six layers of Metglas on both sides of PZT. The red arrows indicate the longitudinal direction of the sensor.

(b) a picture of a Metglas-PZT laminate along with the ID electrode and kapton tape as indicated.

We then characterized the ME response of our laminate structures by measuring the voltages induced across the ID electrodes of the PZT fibers with a lock-in amplifier as a function of the dc magnetic bias field H_{dc} and in response to a Helmholtz coil driven ac field of $H_{\mathrm{ac}} = 1$ Oe at a frequency $f = 1$ kHz. Both dc and ac fields were applied along the length of the laminate. The ME voltage coefficient $\alpha_{\mathrm{ME-V}}$ measured as a function of H_{dc} for two, four, and six Metglas layered structures followed a very similar trend, as reported in [4]. Fig. 1(c) shows a representative $\alpha_{\mathrm{ME-V}}$ profile as a function of H_{dc} for a laminate with six Metglas layers on both sides of the PZT layer: this data is illustrative of a high ME response. One can see that $\alpha_{\mathrm{ME-V}}$ increases as the magnetic field is increased, reaches a maximum of 8.5 V/cm-Oe at about $H_{\mathrm{dc}} = 8$ Oe, and then drops off as the magnetic field is increased further. The value of the ME gain has been found to be repeatable in lots of four sensors to $+/-10\%$. The value of the gain might be enhanced by: (i) use of $\mathrm{Pb(Mg_{1/3}Nb_{2/3})O_3 - PbTiO_3}$ single crystal piezoelectric fibers and (ii) improved layer bonding and laminate fabrication methods. We then packaged these laminates in aluminum boxes; optimized the dc magnetic field with permanent magnets to obtain the highest ME response for each sample; and used them with the charge amplifier circuits for noise characterizations as discussed in the next section.

III. Measurement Method and Theory Analysis

A. Basic Circuit

The ME coupling coefficient is the parameter determining the detection capability for a single ME sensor [2], [3], [7], [8]. In fact, there are two types of coefficients that can be used to describe the ME coupling [5]. One is the ME voltage coefficient $\alpha_{\mathrm{ME-V}}$ which presents the relation between the output electric field and the input magnetic field; and the other, known as ME charge coefficient $\alpha_{\mathrm{ME-C}}$, is used to characterize the charge generation capability of the sensor [6]. These two types of coefficients for different structures of ME sensors should be separately considered: in other words, they should be calculated independently in different cases [10].

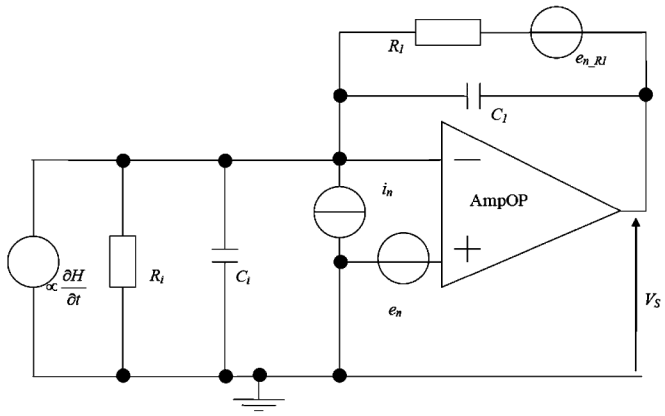

Fig. 2. Basic detection circuit and noise model for ME sensor.

In order to amplify the small signals detected by the ME sensor, we used a charge amplifier (CA) built around a low-noise operational amplifier.

Fig. 2 shows the measurement circuit and the different noise sources. The ME sensor is modeled as a H-induced charge generator: where H is the applied magnetic field, in parallel with a capacitor C_i, and a resistor R_i, which together represent the equivalent sensor parameters. In our experiments, a large feedback resistor $R_1(\approx 10\ \mathrm{G\Omega})$ was used in parallel with the feedback capacitor $C_1(\approx 100\ \mathrm{pF})$ in order to obtain a sufficiently large output voltage. For the low-noise amplifier, we chose LTC6240 (CA1) from Linear Technology: which had an equivalent input noise voltage of $e_n = 7\ \mathrm{nV}/\sqrt{\mathrm{Hz}}$ with a low corner frequency $f_c = 10$ Hz, and an equivalent input noise current of $i_n = 0.6\ \mathrm{fA}/\sqrt{\mathrm{Hz}}$. This setup was used to characterize several "naked" ME sensors. We also studied the noise performances of a series of ME-sensors with a low-frequency electronic LMC6442A referred to here as CA2. It had an equivalent input noise voltage of $e_n = 170\ \mathrm{nV}/\sqrt{\mathrm{Hz}}$ with a low corner frequency $f_c = 0.2$ Hz, and an equivalent input noise current of $i_n = 0.2\ \mathrm{fA}/\sqrt{\mathrm{Hz}}$.

The noise level for the ME sensors and amplifier circuits depended mainly on: i) the environmental noise; ii) the voltage noise $\mathrm{e_n}$ and current noise $\mathrm{i_n}$ of the amplifier, and iii) the thermal noise from the resistor R_1 and the sensor resistance R_i.

B. Theory Noise Analysis

As we pointed above, the output electric noise level for the circuit (see Fig. 2) is mainly dominated by the resistors R_1 and R_i, the amplifier voltage noise e_n, and the current noise i_n. In addition, the transfer function is another important factor for a ME sensor, since a higher transfer function can improve the signal-to-noise ratio (SNR) [8].

The transfer function in (V/T) can be written as

$$T_r(f) = \frac{\alpha_{\mathrm{ME}}(f)}{C_1}\left(\frac{j(2\pi f)R_1C_1}{1 + j(2\pi f)R_1C_1}\right) \qquad (1)$$

where the ME charge coefficient $\alpha_{\rm ME}(f)$ (at an optimal magnetic bias field working point, H_{dc}) is given in (C/T). This transfer function can be simplified in the system bandwidth as

$$T_r(f) \approx \frac{\alpha_{\rm ME}(f)}{C_1}. \quad (2)$$

Furthermore, the total output voltage noise power spectral density in $(\mathrm{V}^2/\mathrm{Hz})$ is

$$e^2_{n\_T}(f) = |Z_1|^2 \left[i^2_{n\_R1}(f) + i^2_n(f)\right] + \left|1 + \frac{Z_1}{Z_i}\right|^2 e^2_n(f) + |T_r(f)|^2 b^2_{n\_sensor}(f) \quad (3)$$

where $i^2_{n\_R1}(f) = e^2_{n\_R1}(f)/R_1^2$, $Z_1 = R_1/(1 + j(2\pi f)C_1R_1)$, $Z_i = R_i/(1 + j(2\pi f)C_iR_i)$, and $b_{n\_sensor}(f)$ represents the equivalent magnetic field noise of the sensor. So, the expected equivalent input magnetic noise power spectral density b^2_n in $(\mathrm{T}^2/\mathrm{Hz})$ is given by

$$\begin{aligned} b^2_{n\_T}(f) &= \frac{e^2_{n\_T}(f)}{|T_r(f)|^2} \\ &= b^2_{n\_R1}(f) + b^2_{n\_in}(f) + b^2_{n\_en}(f) \\ &\quad + b^2_{n\_sensor}(f) \end{aligned} \quad (4)$$

where $b_{n\_R1}, b_{n\_in}, b_{n\_en}$ represent the equivalent magnetic noise of R_1, i_n, and e_n, respectively.

If we neglect the equivalent magnetic sensor noise b_{n_sensor} and if we assume that $R_i \gg R_1$, then the lowest expected magnetic noise can be rewritten as

$$b^2_{n\_T}(f) \approx \frac{1}{\alpha^2_{\rm ME}(f)} \left[\frac{1}{(2\pi f)^2}\left(\left(i^2_n(f) + \frac{e^2_n(f)}{R_1^2} + \frac{4k_bT}{R_1}\right) + (C_i + C_1)^2 e^2_n(f)\right]\right] \quad (5)$$

where all the elements are given in Fig. 2. In the system bandwidth, we have compared theoretical results to measurements presented in the following sections. This comparison shows that the present white noise limit is given by b_{n_en} and $1/f$ noise. White and 1/f noises are mainly limited by

$$b_{n\_T}(f) \approx \frac{(C_i + C_1)}{\alpha_{\rm ME}(f)} e_n(f) \quad (6)$$

and

$$b_{n\_T}(f) \approx \frac{1}{2\pi\,|\alpha_{\rm ME}(f)|\, f}\sqrt{i^2_n(f) + \frac{e^2_n(f)}{R_1^2} + \frac{4k_BT}{R_1}} \quad (7)$$

values, respectively. The second one gives a $1/f$ magnetic noise limit of

$$\frac{i^2_n(f)}{(2\pi f)^2 \alpha^2_{\rm ME}(f)} \quad (8)$$

if $i^2_n(f) > ((e^2_n(f)/R_1^2) + (4k_BT/R_1))$ or $R_1 > (4k_BT/i^2_n(f))$. We can expect, at 1 Hz, a magnetic noise of

$$b_{n\_T}(f)|_{f=1\ \rm Hz} = \frac{i_n(f)}{2\pi f\,|\alpha_{\rm ME}(f)|}. \quad (9)$$

TABLE I
EVOLUTION OF DETECTION PERFORMANCE

	Sensor	*Circuit*
at high frequency	highest $\alpha_{ME\text{-}C}$ lowest C_i	lowest e_n & C_I
at low frequency	highest $\alpha_{ME\text{-}C}$	lowest i_n & C_I highest R_I

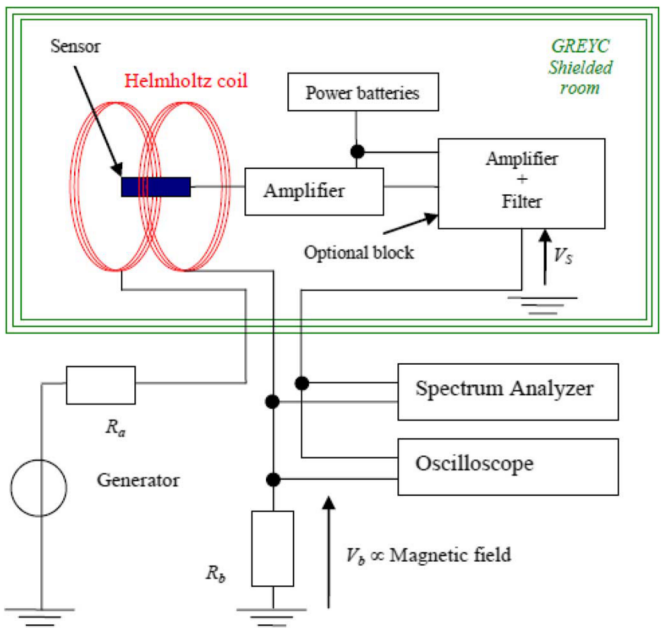

Fig. 3. Experimental measurement schemes.

Around sensor resonant frequency, $f_{Res\_ME} = 30$ kHz, the expected noise limitation is written as

$$b_{n\_T}(f_{Res\_ME}) = (C_i + C_1)\frac{e_n(f_{Res\_ME})}{|\alpha_{\rm ME}(f_{Res\_ME})|}. \quad (10)$$

Table I gives recommendations about how to choose sensor and circuit elements to realize good performance at low or high frequency. In any case, a large ME charge coefficient $\alpha_{\rm ME-C}$ and a small feedback capacitor C_1 in circuit are necessary. We can also see that adaptation between the sensor and circuit design is important.

IV. Experimental Results and Discussion

Sensors were excited by using a Helmholtz coil along the length direction. A pair of permanent magnets attached on two ends of the sensors was used to fix the sensor working point. A generator with a resistor R_a (10 kΩ) generated a current as an input for the Helmholtz coil, and an analyzer (HP 3562A) was used to measure the output signals. Another resistor R_b (10 Ω) was used in the input chain as well to avoid a frequency response influence from the Helmholtz coil. An oscilloscope was used to observe the output temporal signals of the sensor. The Helmholtz coil, amplifier circuit, and another optional preamplifier (EG&G 5113 PRE-AMP) were placed in the GREYC shielded room, as shown in Fig. 3. The equivalent sensor capacitors were 0.37, 0.3, and 0.29 nF for sensor 1, 2, and 3, respectively, which are measured by using a capacitor analyzer (Keithley 590 CV analyzer).

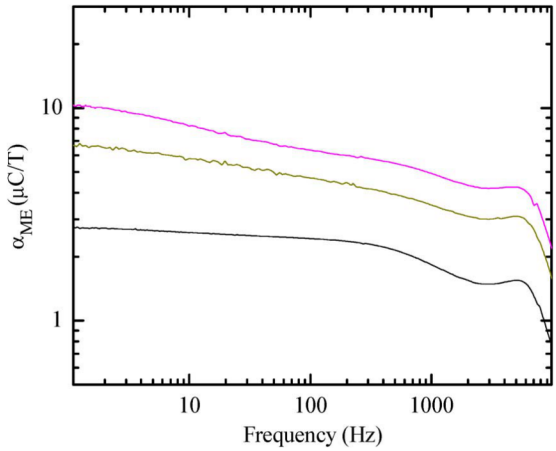

Fig. 4. Charge coefficients, α_{ME}, of three sensors, sensor 1 (black curve), sensor 2 (dark yellow curve), and sensor 3 (pink curve) as a function of frequency and at an optimal magnetic bias field working point, H_{dc}.

A. *Charge Coefficient* $\alpha_{ME}(f)$

The charge coefficients α_{ME-C} of the three sensors were measured at an optimal magnetic bias field working point, H_{dc}, by using a current preamplifier (EG&G 5182) with a transfer function of 100×10^6 A/V, in a low-noise configuration (0.5–1 MHz). In Fig. 4, the three curves represent the charge coefficients of sensor 1, sensor 2, and sensor 3, respectively. Sensor 1 was made of two layers of Metglas with one layer of PZT fibers sandwiched in the middle of them, which were also laminated with ID electrodes on the surface. Sensor 2 was made with similar materials as sensor 1, but the latter had four layers of Metglas on each side of the PZT fibers. Accordingly, its ME coupling was stronger than the sensor 1. Sensor 3 had six layers of Metglas on each side of the PZT fibers to which they were laminated [4]: this third sensor had the last one's charge coefficient almost three times larger than the first one. Sensors 1, 2, and 3 had a charge transfer abilities of 2.7 μT/C, 6.3°μC/T, and 10°μC/T at 1 Hz, respectively.

B. *Transfer Function*

The transfer function describes the magnetic field harvesting ability of a sensor. In general, a high value of the transfer function can reduce the equivalent magnetic noise level.

In Fig. 5(a), because of the increase of the transfer function for the sensor and of the decrease of the transfer function for the circuitry in frequency, the total transfer function is nearly a linear line with frequency at low frequencies. The values were 2.7×10^4 V/T, 6.3×10^4 V/T, and 10^5 V/T for sensors 1, 2, and 3, respectively: which we can calculate by using (2). This confirms the evaluated results predict in Section III.

However, near the sensor's resonant frequency, the ME coupling of the sensors were 10–20 times stronger than that at lower subresonant frequencies, as shown in Fig. 5(b). Due to this strong enhancement in the coupling at the resonant frequency, the equivalent magnetic noise was decreased to the fT/$\sqrt{\text{Hz}}$ level.

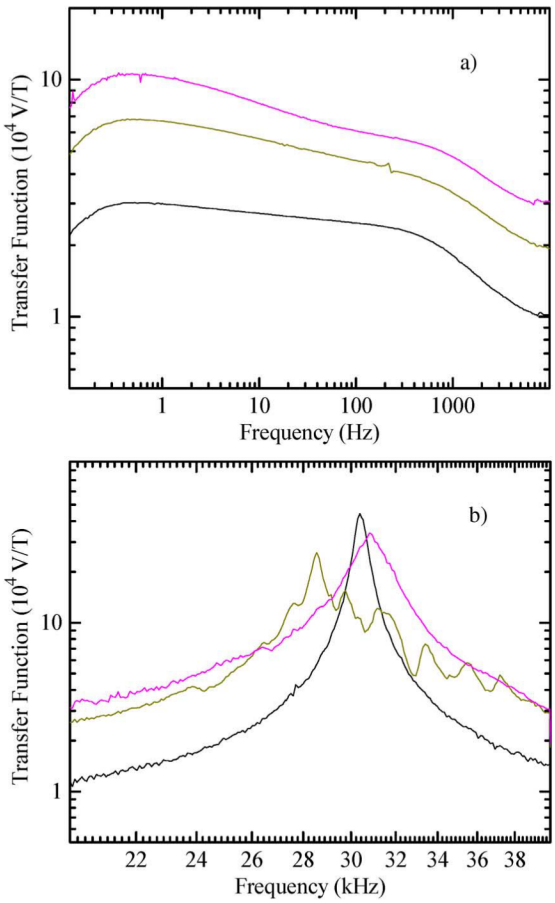

Fig. 5. Transfer function of sensor 1 (black curve), sensor 2 (dark yellow curve), and sensor 3 (pink curve) as a function of frequency, in a large frequency range a) and around the resonance frequency b), by using CA1 with $R_1 = 10$ GΩ, $C_1 = 100$ pF.

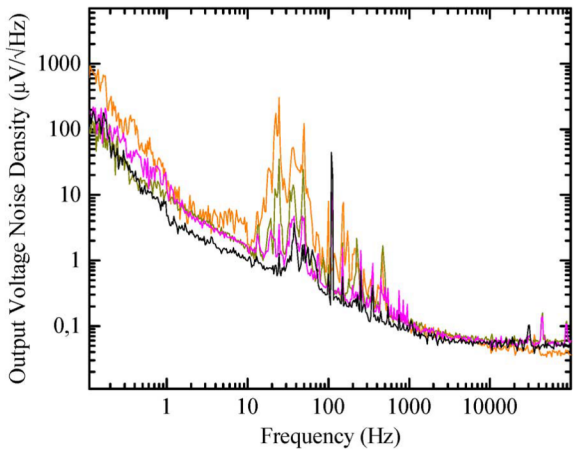

Fig. 6. Output voltage noise density for sensor 1 (black curve), sensor 2 (dark yellow curve), sensor 3 (pink curve) and PZT layer (orange curve) as a function of frequency by using CA1 with $R_1 = 10$ GΩ, $C_1 = 100$ pF.

C. *Output Noise and Equivalent Magnetic Noise Levels*

In Fig. 6, we see that the output voltage noises of these three sensors are nearly at the same level, which is close to the measured one with a single PZT layer as the input of the circuit.

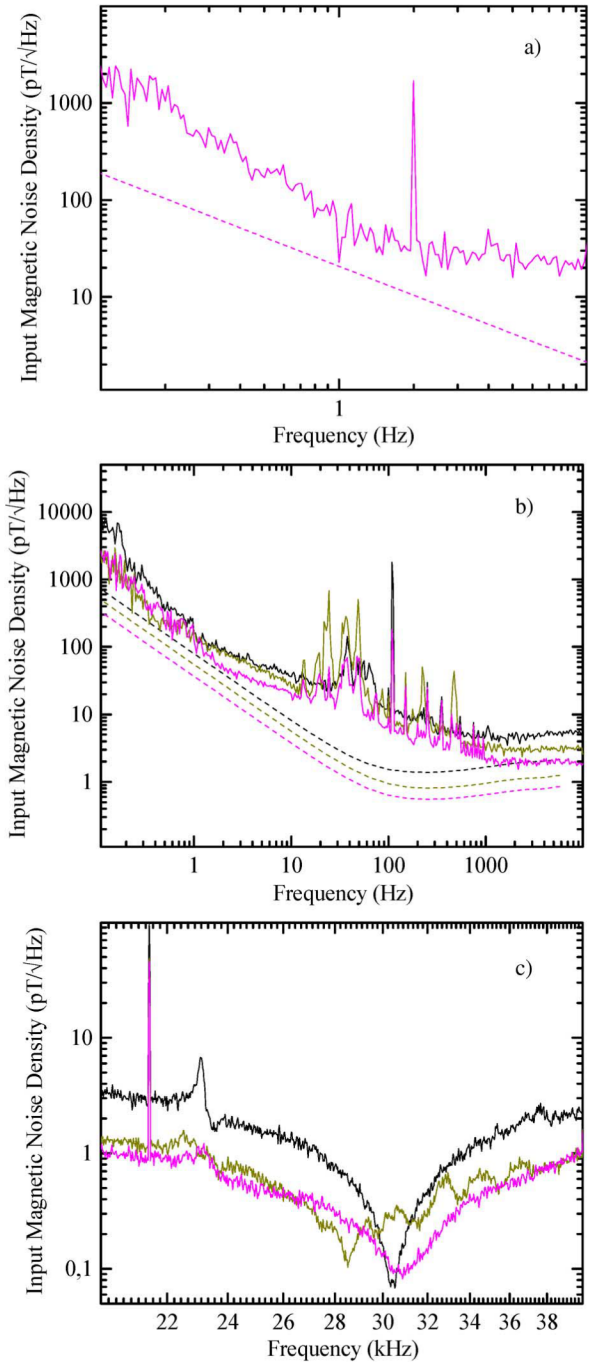

Fig. 7. Measured (solid lines) and calculated (dashed lines) equivalent magnetic noise levels for sensor 1 (black curve), sensor 2 (dark yellow curve), and sensor 3 (pink curve) as a function of frequency (a) by using CA2 in small bandwidth with $R_1 = 10$ GΩ, $C_1 = 100$ pF, (b-c) by using CA1, with $R_1 = 10$ GΩ, $C_1 = 100$ pF, in large bandwidth and around the resonant frequencies.

Presently, it means that output electric noise level depends mainly on the PZT layer and the detection circuit.

The second circuit (CA2) gives a very low-level equivalent magnetic noise at low frequencies, as shown in Fig. 7(a). A large bandwidth equivalent magnetic noise was characterized by the circuit (CA1). An extreme low-noise level was found around the sensor's resonant frequency. The calculated equivalent magnetic noise levels are presented as dashed lines with corresponding colors with respect to (5).

TABLE II
MEASURED AND EXPECTED NOISE LEVEL AROUND RESONANT FREQUENCY

	Noise level	*Expected noise level*
Sensor 1	≈ 70 fT/√Hz	70 fT/√Hz
Sensor 2	≈ 110 fT/√Hz	107 fT/√Hz
Sensor 3	≈ 90 fT/√Hz	82 fT/√Hz

The equivalent magnetic noise level reaches a value of 65 $\mathrm{pT}/\sqrt{\mathrm{Hz}}$ at 1 Hz for sensor 3 using the low-noise small bandwidth circuit (CA2), as shown in Fig. 7(a). A $\mathrm{fT}/\sqrt{\mathrm{Hz}}$ level for the equivalent magnetic noise was found near 30 kHz. Table II shows the experimental and calculated equivalent magnetic noise levels near the resonant frequency.

V. CONCLUSION

The performance of Metglas/PZT fiber ME laminates have been characterized by using a low-noise detection charge amplifier. Analysis was performed with an equivalent model, which predicted impressive low equivalent magnetic noise levels at low frequencies, and an extremely low equivalent magnetic noise level near the electromechanical resonant frequency for the given ME sensor. We can conclude that: i) The ME charge coefficient is the most important factor for a single ME sensor, both large and small bandwidth performances are directly dominated by this factor. ii) The bandwidth and noise performances of ME sensors are mainly due to the input current noise level of the amplifier used and the feedback elements of the charge amplifier, respectively. If the feedback resistor is big enough (e.g., much bigger than 400 GΩ), the low-frequency equivalent magnetic noise is, in theory, proportional to the input current noise level of the amplifier, i_n, circuit. However, sensor noise as an equivalent magnetic noise, b_{n_sensor}, should also be considered in the low-frequency range as well. Its origin and associated limitation will be further detailed. We notice that this equivalent noise level seems to appear in some curves (cf. Fig. 7) as 1/f noise. Meanwhile, it is to close to the present electronics noise limitations: thus, we are not able to conclude with confidence and it remains to be better clarified later. iii) For large bandwidth sensors, the performance is dominated by the equivalent capacitance of the ME sensors, the input voltage noise, and the feedback capacitor of the charge amplifier used.

REFERENCES

[1] C.W. Nan, "Magnetoelectric effect in composites of piezoelectric and piezomagnetic phases," *Phys. Rev. B*, vol. 50, no. 9, pp. 6082–6088, Sep. 1994.

[2] S. Dong, J. Li, and D. Viehland, "Longitudinal and transverse magnetoelectric voltage coefficients of magnetostrictive/piezoelectric laminate composite: Theory," *IEEE Trans. Ultrason. Ferroelect. Freq. Control*, vol. 50, no. 10, pp. 1253–1261, Oct. 2003.

[3] S. Dong, J. Li, and D. Viehland, "Longitudinal and traverse magnetoelectric voltage coefficients of magnetostrictive/piezoelectric laminate composite: Experiments," *IEEE Trans. Ultrason., Ferroelect. Freq. Control*, vol. 51, no. 7, pp. 793–798, 2004.

[4] J. Das, J. Gao, Z. Xing, J. F. Li, and D. Viehland, "Enhancement in the field sensitivity of magnetoelectgric laminate heterostrures," *Appl. Phys. Lett.*, vol. 95, p. 092501, 2009.

[5] S. Dong, J. Zhai, J. Li, and D. Viehland, "Near-ideal magnetoelectricity in high-permeability magnetostrictive/piezofiber laminates with a (2-1) connectivity," *Appl. Phys. Lett.*, vol. 89, p. 252904, 2006.

[6] S. Dong, J. Zhai, Z. Xing, J. Li, and D. Viehland, "Giant magnetoelectric effect (under a dc magnetic bias of 2 oe) in laminate composites of febsic alloy robbons and $\mathrm{pb}(\mathrm{zn}_{1/3}, \mathrm{nb}_{2/3})\mathrm{o}_3 - 7\%\mathrm{pbtio}_3$ fibers," *Appl. Phys. Lett.*, vol. 91, p. 022915, 2007.

[7] Z. Xing, J. Zhai, S. Dong, J. Li, D. Vieland, and W. Odendaal, "Modeling and detection of quasi-static nanotesla magnetic field variations using magnetoelectric laminates sensors," *Meas. Sci. Technol.*, vol. 19, p. 015206, 2008.

[8] Z. Xing, J. Li, and D. Viehland, "Modeling and the signal-to-noise ratio research of magnetoelectric sensors at low frequency," *Appl. Phys. Lett.*, vol. 91, no. 14, p. 142905, 2007.

[9] C. D. Motchenbacher and J. A. Connelly, *Low-Noise Electronic System Design*. New York: Wiley, Jun. 1993, pp. 38–68.

[10] Z. Xing, J. Zhai, J. Gao, J. Li, and D. Viehland, "Magnetic-Field sensitivity enhancement by magnetoelectric sensor arrays," *IEEE Electron Device Lett.*, vol. 30, no. 5, pp. 445–447, May 2009.